Computational study of Electron Paramagnetic Resonance parameters for Mg and Zn impurities in β-Ga_2O_3

Dmitry Skachkov* and Walter R. L. Lambrecht
Department of Physics, Case Western Reserve University, 10900 Euclid Avenue, Cleveland, OH-44106-7079, U.S.A.

A computational study of the electron paramagnetic resonance (EPR) g-tensors and hyperfine tensors in Mg and Zn doped β-Ga_2O_3 is presented. While Mg has been found previously to prefer the octahedral site, we find here that Zn prefers the tetrahedral substitutional site. The EPR signatures are found to be distinct for the two sites. Good agreement with experiment is found for the g-tensor and hyperfine interaction for Mg_{Ga2} and predictions are made for the Zn case.

Monoclinic β-Ga_2O_3 with a band gap of about 4.7±0.1 eV,[1–5] has recently attracted attention as an ultra-wide-band-gap semiconductor for transistor and transparent conducting applications.[6,7] As for any semiconductor, a thorough understanding of the defects and dopants and ultimately their control is crucial to the development of this material. Several previous theoretical works have addressed the point defects.[8–15] On the experimental side, Electron Paramagnetic Resonance (EPR) provides one of the most powerfull methods to identify the chemical nature of defect centers. Several papers recently reported EPR centers in β-Ga_2O_3.[16–21]

In this paper we address the recently reported Mg_{Ga} acceptor type dopant.[18] We present first-principles calculations of the g-tensor and hyperfine parameters characteristic of this defect, which support the previous assignment of this defect with the Mg on the octahedral Ga site. In fact, we present calculations for both sites and show that they would be distinctly different. Previous computational work[20] indeed finds Mg to have lower energy on the octahedral site. Encouraged by this agreement with experiment, we then consider another candidate acceptor, Zn_{Ga} and predict its EPR signatures. Our reason for choosing Zn is that Zn may prefer the tetrahedrally coordinated site. In fact, Mg in MgO occurs in a rocksalt structure with octahedral environment but Zn in ZnO has a tetrahedral bonding. Thus we anticipated that Zn might prefer the tetrahedral site in β-Ga_2O_3. We will show that this hypothesis is confirmed and predict the corresponding g-tensor and hyperfine splittings.

The g-tensor is calculated using the Gauge Including Projector Augmented Wave (GIPAW) method.[22–25] This is a Density Functional Perturbation Theory (DFPT) method to calculate the linear magnetic response of a periodic system onto an external magnetic field. It is implemented in the code QE-GIPAW,[26] which is integrated within the Quantum Espresso package.[27]

The hyperfine tensor calculation is also incorporated in the GIPAW code although it does not strictly require the GIPAW methodology. The hyperfine tensor has two parts: the isotropic Fermi contact term which depends on the wave function or spin density of the defect at the nuclear sites of atoms with a net nuclear spin and a dipole interaction term which is non-isotropic. The hyperfine interaction is sensitive to the degree of localization of the defect wave fuctions. The latter tends to be underestimated by the local density approximation (LDA) or even generalized gradient approximation (GGA) to the exchange-correlation functional, particularly for acceptors. This is because the latter does not fully cancel the Coulomb self-interaction. This can in part be remedied by using an orbital dependent functional such as a hybrid functional or in a less expensive manner using DFT+U, in which on-site orbital specific Coulomb interactions are added. These have the effect of shifting empty states (hole states) up in energy and deeper in the gap, thereby making them more localized. Typically, this also involves a feedback in the relaxation of the structure which then tends to become localized on a single atom instead of spreading of the several nearest neighbors of a defect site.

In the case of β-Ga_2O_3 the acceptor states tend to be localized on O-p like dangling bonds because these comprise the top of the valence band. In previous works[19,21] on the EPR parameters of Ga-vacancy related states, we found it was necessary to apply a rather large U on O-p states, in order to obtain adequate localization on their neighboring O atoms and reduce the s-like spin density on the second neighbor which determines the superhyperfine (SHF) interaction. Within pure semi-local functionals, the SHF interaction on the Ga neighbors to the O on which the spin density becomes localized was overestimated by almost a factor 2 even if the structure was relaxed with DFT+U or hybrid functional. On the other hand, Ho *et al.*[20] showed that using a hybrid functional, the Mg_{Ga} acceptor —which has its spin density localized on a nearby O and is thus in many ways similar to the vacancies— good agreement was obtained between theory and experiment for the strength of the hyperfine coupling. Here we will show that this is the case also in pure GGA provided the structure is relaxed using GGA+U. This is because the defect spin density is then already very well localized on a single O and not as sensitive to the U value.

At present, the GIPAW code does not yet allow us to calculate the g-tensor using electronic structures at the DFT+U or hybrid functional level. Thus our g-tensor calculations are performed at the GGA level using the Perdew-Burke-Ernzerhof[28] functional but using structures relaxed in DFT+U.

We consider Mg_{Ga1} (tetrahedral) as well as Mg_{Ga2} (oc-

TABLE I. Calculated EPR parameters for Mg_{Ga} and Zn_{Ga} defects. In our results the g tensor and A-tensors are given in terms of three principal values followed by the θ (polar) and ϕ (azimuthal) angles in degrees measured from **b** and $\mathbf{a}_*$ respectively. The results of other groups pertain to Mg_{Ga2} and give the g and A for magnetic field along **a** ,**b**, **c**.

Model		g-tensor			HFI $Ga_{(1)}$ A (G)			HFI $Ga_{(2)}$ A (G)			HFI Mg/Zn A (G)		
Mg_{Ga1}		2.0096	2.0241	2.0205				14.98	15.26	14.76	3.26	3.21	2.54
	θ	90	0	90				85	41	49	90	0	90
	ϕ	14		-76				-9	76	86	-25		65
Mg_{Ga2}		2.0088	2.0222	2.0271	19.90	19.02	18.39	12.73	12.64	13.03	1.94	1.43	2.03
	θ	85	13	78	88	8	83	77	41	52	78	42	50
	ϕ	23	-45	-68	27		-64	-32	74	48	-8	-84	72
Zn_{Ga1}		2.0089	2.0078	2.0190				15.58	15.32	15.90	7.88	6.74	3.68
	θ	89	0	90				89	46	44	90	0	90
	ϕ	-1		-89				-10	80	81	-9		81
Zn_{Ga2}		2.0125	2.0207	2.0330	17.14	17.30	18.06	12.44	12.72	12.34	11.83	3.77	9.90
	θ	41	52	77	58	43	64	78	50	42	85	43	47
	ϕ	29	3	-77	-25	-73	48	-21	78	55	-8	87	77
		a	b	c	a	b	c	a	b	c			
HSE[20]					27.2	28.9	25.7	14.4	14.7	14.2			
Expt.[18]		2.0038	2.0153	2.0371	26.1	25.6	25.5	11.8	11.9	11.3			

tahedral) sites although previous work has already shown that the octahedral site has lower energy and calculate their EPR relevant properties in the neutral charge state. The calculated g-tensors principal values and axes as well as the SHF splitting A tensor are given in Table I. Their corresponding spin-densities for both sites are shown in Fig. 1 as yellow isosurfaces along with the tensor principal axes, shown as arrows and the highlighted atoms on which there is significant SHF interaction. In previous work[18,20] the g tensor and A-tensor values were presented along **a** instead of $\mathbf{a}_*$, but strictly speaking the three principal axes should be orthogonal to each other and the tensor is only fully specified by giving the values along the three principal axes, and the directions of the latter. The calculated principal axes are close to but not exactly along the mutually orthogonal directions $\mathbf{a}_*$ (*i.e.* the direction of the reciprocal lattice vector), **b** and **c**. The angle between **c** and **a** is 103.7°, so $\mathbf{a}_*$ and **a** differ by 13.7° only, so this does not make much difference when comparing to the experimental values the way they were specified. For Mg_{Ga2} we obtain $g_c = 2.025$, $g_b = 2.022$ and $g_a = 2.0132$. These values agree in the ordering from small to large with the experimental values. Similar considerations are valid for the A-tensors which are even closer to being isotropic.

We can see in Fig. 1 that for Mg_{Ga1} the principal axes are very close to the crystal axes. However, for Mg_{Ga2}, which is slightly more asymmetric and tilted, they are farther away from the crystal axes. The spin density is in both cases seen to be oriented close to $\mathbf{a}_*$ which is the direction in which the Δg is smallest for both centers.

We can see that for the tetrahedral site, the spin density is well localized on an $O_{(1)}$ next to the Mg on the mirror plane of the crystal structure and with strong SHF interaction on two equivalent octahedral $Ga_{(2)}$ neighbors with a nearly isotropic SHF tensor A. The A-tensor principal axes however are not oriented close to the crystal axes but rather along the octahedral bonds, one of which is along $\mathbf{a}_*$ but the other are nearly 45° tilted from **b** and **c**. In contrast, for the octahedral site, the spin density is still located on $O_{(1)}$ but with hyperfine on two inequivalent Ga neighbors. Again, the A-tensor in the $Ga_{(2)}$ neighbor have their principal axes along the octahedral bonds. For The $Ga_{(1)}$ neighbor one axes is close to **c** along one of the tetrahedral bonds while the other two axes also are close to the tetrahedral bond directions.

The octahedral Mg_{Ga2} site model is in agreement with experimental findings of Kananen *et al.*[18] while the tetrahedral Mg_{Ga1} is not. In terms of the g-tensor there is also good agreement with the Mg_{Ga2} site. For $Ga_{(2)}$ the g-tensor in the "close to" **c** direction is calculated to be slightly higher than in the close to **b** direction, in agreement with experiment, while for Mg_{Ga1} it is the other way around. However, these differences are almost within the errorbars of calculating Δg and it is really the inequivalence of the SHF that is the telltale sign of the octahedral site.

The assignment of the experimental EPR center to Mg_{Ga2} agrees with Ho *et al.* 's[20] finding that the Mg has lower total energy on the octahedral site. Nonetheless, it might not completely exclude some Mg to also occur on tetrahedral sites and thus it might be possible in the future to detect also the Mg_{Ga1} EPR center whose properties are here predicted. In terms of the SHF agreement with experiment, our values with GGA underestimate the experimental values for the $Ga_{(1)}$ by 23% and overestimate the ones for $Ga_{(2)}$ by 10 % while Ho *et al.*[20] overestimates the $Ga_{(1)}$ values by 6 % and the $Ga_{(2)}$ ones by 24 %. In terms of anisotropy of A, neither calculation predicts the ordering of the tensor principal axes components correctly as given by the experiment. However, all calculations agree with experiment that the

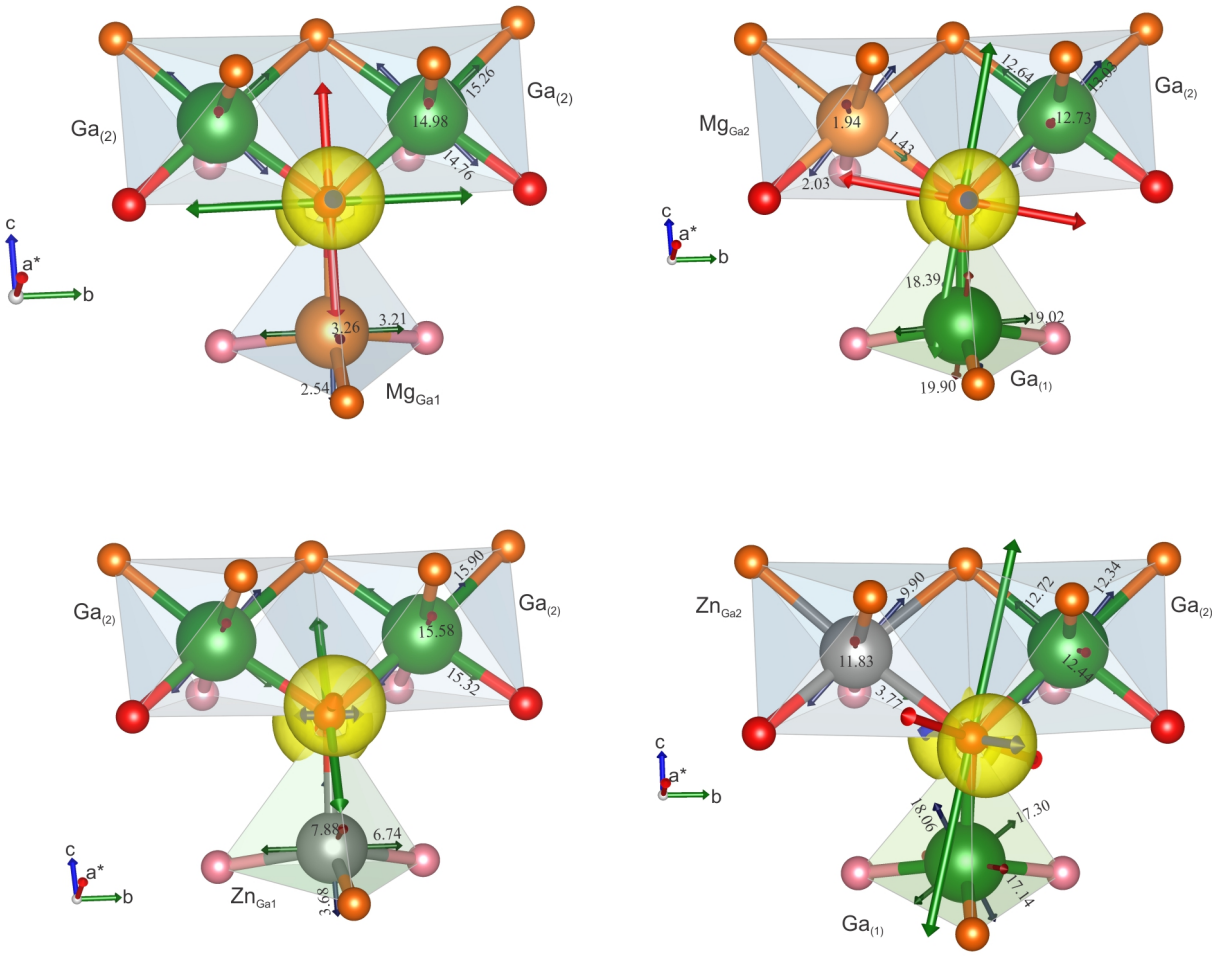

FIG. 1. Mg_{Ga1}, Mg_{Ga2}, Zn_{Ga1}, and Zn_{Ga2} structures, spin density in yellow, g-tensor principal axes indicated by thick double arrows with length proportional to the Δg (deviation from free electron value $g_e = 2.002391$), green colored Ga atoms are the ones with strong SHF interaction. The small O spheres are color coded red $O_{(1)}$, pink $O_{(2)}$, orange $O_{(3)}$ and the polyhedra surrounding the Ga and their type are indicated. The thin double arrows show the principal axes of SHF interaction.

anisotropy is small and hence more or less within the errorbar. Furthermore, the present calculations indicate that the hyperfine tensors have principal axes along the bond direction rather than along the crystal directions but insufficient experimental detail on this is presently given in the experimental paper.[18] Thus there is no clear advantage to the hybrid functional in predicting the EPR parameters, provided the structure is properly relaxed with spin well localized on a single O.

On both sites, this acceptor was found to have a very deep $0/-$ transition level about equal for both sites.[20] They are significantly less deep in GGA than in hybrid functional. Kyrtsos *et al.*[15] find the Mg acceptor level in GGA at 0.26/0.22 eV above the VBM for tetrahedral and octahedral site respectively, while in the hybrid functional calculation, they lie at 1.25 /1.05 eV according to Kyrtsos *et al.* and at 1.62/1.57 eV according to Ho *et al.*[20]. The differences between these two hybrid functional results may stem from different treatment of the image charge corrections, where in one case[15] a static dielectric constant was used for screening and in the other[20] the high-frequency value was used. Slighlty different hybrid functional parameters such as the fraction (α) of exact (non-local) exchange, screened with screening length μ, included ($\alpha = 0.26$, $\mu = 0$)[13,20] vs. ($\alpha = 0.32$, $\mu = 0.2$ Å^{-1})[15] may also play a role. Thus the exact values of these transition levels are still under dispute and have not yet been settled by experiment. In any case these levels lie rather deep below the conduction band minimum (CBM) in β-Ga_2O_3 which is usually unintentionally n-type or at least semi-insulating, and thus they can only be made EPR active by optical excitation removing the electron from the $q = -1$ state.

Next, we consider the Zn_{Ga1} and Zn_{Ga2} acceptors. According to Kyrtsos et al.[15] the $0/-$ transition level for this acceptor lies a bit higher above the VBM than for Mg, at 0.35/0.27 eV (GGA) or 1.39/1.22 eV (hybrid) for the tetrahedral/octahedral site. Again, we calculate their properties in the neutral state only, which is the EPR active state. As we hypothesized, we find that in

this charge state, the tetrahedral site has lower energy than the octahedral site, in fact, by 0.16 eV. The resulting g-tensor and hyperfine tensors are given in Table I and the spin densities and tensors are visualized in Fig.1. These are very similar to the corresponding Mg case but, based on the total energy, we predict in this case that the tetrahedral site should be easier to find experimentally. It would be characterized by hyperfine on two equivalent Ga atoms and a g-tensor with maximum value along **c**. For the Zn_{Ga2} site, the principal axes of the tensor are again somewhat further from the crystal axes. Interestingly, for Zn_{Ga1} the g-tensor has its lowest value along **b** even though the spin density is mostly along $\mathbf{a}_*$ but both values have in fact small deviations from the free electron value. It is also worthwhile pointing out that the highest value of the g-tensor in this case is along the **c** principal axis and two relatively small values are found in the orthogonal directions. It is thus close to the g-tensor previously assigned to a V_{Ga_2},[19,21] which also has two nearly equivalent Ga atoms and with A values close to the ones calculate here. It might thus be difficult to distinguish the Zn_{Ga1} EPR center from the $Ga_{(2)}$ vacancy one. It is however highly unlikely that the samples in the previous experimental studies of Ga-vacancies induced by irradiation would have contained Zn and the Ga-vacancy EPR centers became only visible after high energy particle irradiation which is required to create the vacancies in the first place, because the vacancies have high energy of formation. It would be interesting to search for the here predicted Zn-related EPR center in a sample doped with Zn and without irradiation.

Finally, we mention that Mg and Zn in principle also could show hyperfine splittings from the ^{67}Zn (4.1% abundance) and ^{25}Mg (10 % abundance) isotopes, both corresponding to a $I = 5/2$ nuclear spin. Because of the low abundances, these would be difficult to detect but we nonetheless provide their hyperfine properties in the last columns of Table I. One may see that for Zn, the values are comparable to Ga and show a larger anisotropy.

In summary, we have calculated the EPR signatures of the Mg and Zn acceptors in β-Ga_2O_3 for both candidate sites, the octahedral and tetrahedral one. Based on total energy calculations, the tetrahedral is predicted to be preferred for the Zn, while the octahedral site is preferred for Mg. Both sites are shown to have distinct EPR signatures and the predictions agree well with experiment for the Mg case. Our results also show that hybrid functional calculations are not clearly providing improved hyperfine splitting parameter results compared to GGA calculations. Nonetheless some type of orbital dependent functional, hybrid or DFT+U is required to obtain a correctly relaxed structure with spin localized on one oxygen. In terms of the hyperfine tensors, we find that their principal axes occur close to the octahedral and tetrahedral bond directions rather than along the crystalline axes.

This work was supported by the National Science Foundation (NSF), Division of Materials Research (DMR) under grant No. 1755479. The calculations were done at the Ohio Supercomputer Center under Project No. PDS0145.

* Corresponding author dmitry.skachkov@case.edu

[1] T. Matsumoto, M. Aoki, A. Kinoshita, and T. Aono, Jap. J. Appl. Phys. **13**, 1578 (1974).

[2] H. Peelaers and C. G. Van de Walle, Phys. Status Solidi (b) **252**, 828 (2015).

[3] J. Furthmüller and F. Bechstedt, Phys. Rev. B **93**, 115204 (2016).

[4] K. A. Mengle, G. Shi, D. Bayerl, and E. Kioupakis, Appl. Phys. Lett. **109**, 212104 (2016), http://dx.doi.org/10.1063/1.4968822.

[5] A. Ratnaparkhe and W. R. L. Lambrecht, Applied Physics Letters **110**, 132103 (2017), http://dx.doi.org/10.1063/1.4978668.

[6] K. Sasaki, M. Higashiwaki, A. Kuramata, T. Masui, and S. Yamakoshi, J. Cryst. Growth **378**, 591 (2013), the 17th International Conference on Molecular Beam Epitaxy.

[7] A. J. Green, K. D. Chabak, E. R. Heller, R. C. Fitch, M. Baldini, A. Fiedler, K. Irmscher, G. Wagner, Z. Galazka, S. E. Tetlak, A. Crespo, K. Leedy, and G. H. Jessen, IEEE Electron Device Letters **37**, 902 (2016).

[8] J. B. Varley, H. Peelaers, A. Janotti, and C. G. Van de Walle, J. Phys. Condens. Matter **23**, 334212 (2011).

[9] J. B. Varley, A. Janotti, C. Franchini, and C. G. Van de Walle, Phys. Rev. B **85**, 081109 (2012).

[10] T. Harwig and F. Kellendonk, J. Solid State Chem. **24**, 255 (1978).

[11] T. Zacherle, P. C. Schmidt, and M. Martin, Phys. Rev. B **87**, 235206 (2013).

[12] H. Peelaers and C. G. Van de Walle, Phys. Rev. B **94**, 195203 (2016).

[13] P. Deák, Q. D. Ho, F. Seemann, B. Aradi, M. Lorke, and T. Frauenheim, Phys. Rev. B **95**, 075208 (2017).

[14] A. Kyrtsos, M. Matsubara, and E. Bellotti, Phys. Rev. B **95**, 245202 (2017).

[15] A. Kyrtsos, M. Matsubara, and E. Bellotti, Applied Physics Letters **112**, 032108 (2018), https://doi.org/10.1063/1.5009423.

[16] B. E. Kananen, L. E. Halliburton, K. T. Stevens, G. K. Foundos, and N. C. Giles, Applied Physics Letters **110**, 202104 (2017), http://dx.doi.org/10.1063/1.4983814.

[17] B. E. Kananen, N. C. Giles, L. E. Halliburton, G. K. Foundos, K. B. Chang, and K. T. Stevens, Journal of Applied Physics **122**, 215703 (2017), https://doi.org/10.1063/1.5007095.

[18] B. E. Kananen, L. E. Halliburton, E. M. Scherrer, K. T. Stevens, G. K. Foundos, K. B. Chang, and N. C. Giles, Applied Physics Letters **111**, 072102 (2017), https://doi.org/10.1063/1.4990454.

[19] H. J. von Bardeleben, S. Zhou, U. Gerstmann, D. Skachkov, W. R. L. Lambrecht, Q. D. Ho,

and P. Deák, APL Materials **7**, 022521 (2019), https://doi.org/10.1063/1.5053158.
[20] Q. D. Ho, T. Frauenheim, and P. Deák, Journal of Applied Physics **124**, 145702 (2018), https://doi.org/10.1063/1.5049861.
[21] D. Skachkov, W. R. L. Lambrecht, H. J. von Bardeleben, U. Gerstmann, Q. D. Ho, and P. Deák, J. Appl. Phys. **125**, ? (2019), in press, arXiv:1808.05652.
[22] C. J. Pickard and F. Mauri, Phys. Rev. B **63**, 245101 (2001).
[23] C. J. Pickard and F. Mauri, Phys. Rev. Lett. **88**, 086403 (2002).
[24] U. Gerstmann, M. Rohrmüller, F. Mauri, and W. Schmidt, Physica Status Solidi (c) **7**, 157 (2010).
[25] D. Ceresoli, U. Gerstmann, A. P. Seitsonen, and F. Mauri, Phys. Rev. B **81**, 060409 (2010).
[26] `http://qe-forge.org/gf/project/qe-gipaw/`.
[27] P. Giannozzi, S. Baroni, N. Bonini, M. Calandra, R. Car, C. Cavazzoni, D. Ceresoli, G. L. Chiarotti, M. Cococcioni, I. Dabo, A. Dal Corso, S. de Gironcoli, S. Fabris, G. Fratesi, R. Gebauer, U. Gerstmann, C. Gougoussis, A. Kokalj, M. Lazzeri, L. Martin-Samos, N. Marzari, F. Mauri, R. Mazzarello, S. Paolini, A. Pasquarello, L. Paulatto, C. Sbraccia, S. Scandolo, G. Sclauzero, A. P. Seitsonen, A. Smogunov, P. Umari, and R. M. Wentzcovitch, Journal of Physics: Condensed Matter **21**, 395502 (19pp) (2009).
[28] J. P. Perdew, K. Burke, and M. Ernzerhof, Phys. Rev. Lett. **77**, 3865 (1996).

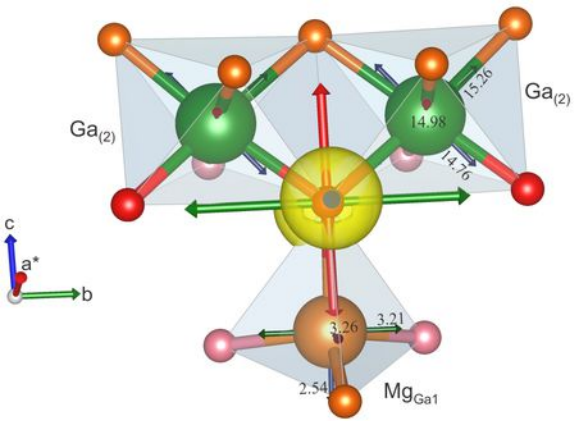
Ga(2)
Ga(2)
14.98
15.26
14.76
c
a*
b
3.26
3.21
2.54
MgGa1

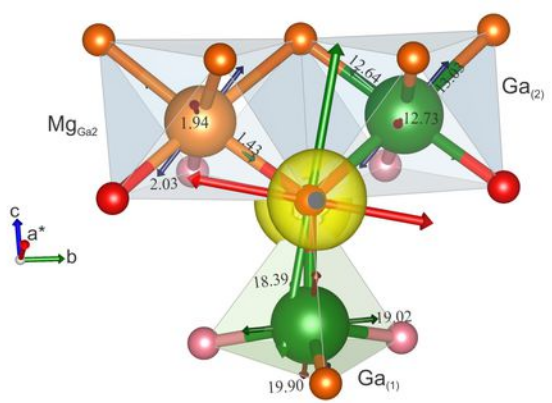
MgGa2
Ga(2)
1.94
12.64
12.73
1.43
2.03
c
a*
b
18.39
19.02
19.90
Ga(1)

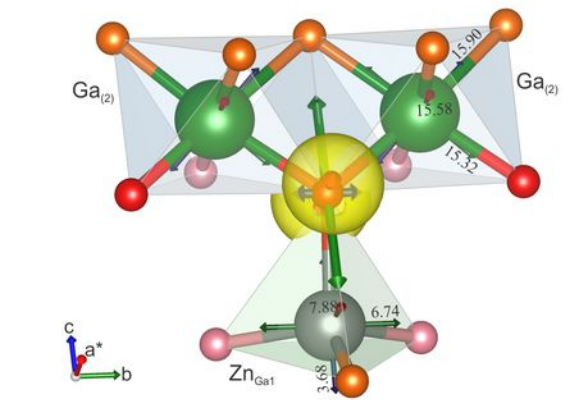
Ga(2)
Ga(2)
15.90
15.58
15.32
c
a*
b
7.88
6.74
ZnGa1
3.68

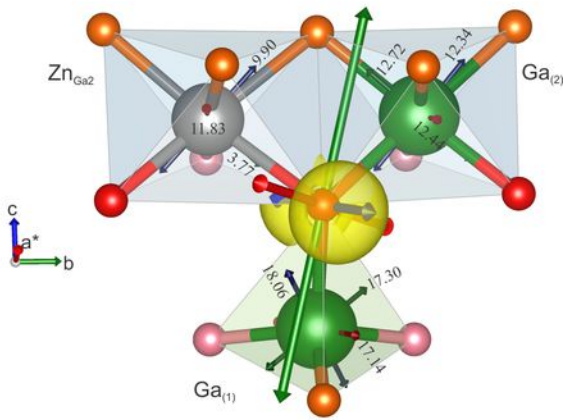
ZnGa2
Ga(2)
9.90
12.72
12.34
11.83
12.44
3.77
c
a*
b
18.06
17.30
17.14
Ga(1)